Pergamon

0045-7930(94)00018-2

*Computers Fluids* Vol. 23, No. 8, pp. 983–1004, 1994

0045-7930/94 $7.00 + 0.00

# ASSESSMENT OF TURBULENCE-TRANSPORT MODELS INCLUDING NON-LINEAR RNG EDDY-VISCOSITY FORMULATION AND SECOND-MOMENT CLOSURE FOR FLOW OVER A BACKWARD-FACING STEP

F. S. LIEN and M. A. LESCHZINER
University of Manchester Institute of Science and Technology (UMIST), Manchester M60 1QD, U.K.

*(Received 29 November 1993; in revised form 4 May 1994)*

**Abstract**—A computational study is performed in which the predictive capabilities of a range of eddy-viscosity and second-moment-closure models are examined by reference to a separated flow behind a backward-facing step in an expanding channel. The models include three second-moment-closure variants, all being of the 'Launder–Reece–Rodi' type, two RNG $k$–$\epsilon$ forms, one combining the RNG approach with a non-linear eddy-viscosity formulation, and a low-Re $k$–$\epsilon$ model. The study demonstrates that to achieve a solution similar to that returned by second-moment closure, the RNG formulation needs to be implanted into a non-linear eddy-viscosity framework; neither returns, on its own, the correct behaviour, not even for mean-flow features. Moreover, relatively minor variations within second-moment closure—specifically, such relating to wall-induced effects on turbulence isotropisation and to stress diffusion—can significantly alter the overall performance of the closure. All models specifically designed to return realistic solutions for normal stresses seriously over-estimate anisotropy.

## 1. INTRODUCTION

Separation, recirculation and reattachment are features encountered in numerous practical situations. They occur whenever a fast-flowing fluid is required to bypass an obstacle or whenever a confining wall undergoes a rapid change in orientation to form a strongly curved convex surface. Recirculation has profound consequences in relation to pressure recovery, pressure drag, wall friction and heat-transfer characteristics. It is also a powerful generator of turbulence and hence mixing and losses. Separated flows have thus naturally been the subjects of many studies, both experimental and computational.

The objectives pursued in different studies have varied considerably. Frequently, however, the general emphasis has been on understanding and capturing the separation process, particularly if this occurred on a curved surface, on resolving the structure of the separated shear layer and the recirculation zone it envelops, on describing the location of reattachment and the dominant processes in the reattachment region, and on understanding and predicting the processes governing the flow recovery in the wake region following reattachment. All these issues are sufficiently fundamental to be common to the majority of practical as well as idealised laboratory flows, and it is on the latter type of flows that studies tended to concentrate, if only because of the availability of experimental data suitable for validation. For example, particularly extensive and accurate experimental data for backward-facing-step flow have been obtained by Kim *et al.* [1], Eaton and Johnson [2] and Driver and Seegmiller [3].

When a flow separates, a curved and highly turbulent free shear layer is formed first. In this layer, turbulence anisotropy will not generally be as large as in the boundary layer preceding separation, yet this anisotropy can have a much greater influence on mean-flow characteristics than that in the parent boundary layer. This is due, principally, to the strong interaction between curvature strain and the normal stresses, on the one hand, and the sensitivity of the shear stress to normal stress anisotropy, on the other. Specifically, curvature tends to attenuate the shear stress and hence the level of fluid entrainment into the shear layer—an interaction which dictates the intensity of curvature in the shear layer and hence the reattachment position. Additionally, gradients of normal stresses (expressed in terms of directionally invariant components in a fixed frame of reference) contribute significantly to momentum transport. As the flow approaches reattachment, it is

subjected to severe normal strain, yet this can be shown not to contribute measurably to the turbulence-generation process; here too, normal-stress anisotropy plays a crucial role. Apart from provoking severe flow curvature, associated with the impingement process, the wall tends to attenuate turbulent fluctuations normal to it and to enhance wall-parallel components, the result being a particularly high level of normal-stress anisotropy. Finally, within the recirculation zone, curvature is high and affects the turbulence structure through the same mechanism identified above in relation to the free shear layer following separation.

The above complex processes—in particular the important role played by anisotropy—has provided a powerful argument for using second-moment closure (Reynolds-stress models) for resolving separated flows, and this route has been followed vigorously over the past decade by several research groups, particularly in the U.K., France, the U.S.A. and Japan. While related studies have yielded ample evidence for the predictive superiority of second-moment closure over eddy-viscosity models in respect of a significant number of complex flows and flow features, several studies have also demonstrated important defects. Thus, specifically for the case of flow behind a backward-facing step, studies by Kadja [4], Lin [5], Sebag and Laurence [6], Lasher and Taulbee [7] and Obi *et al.* [8] have highlighted excessive levels of anisotropy, inappropriately low rates of wake recovery following reattachment and a physically unrealistic reattachment process as being the principal weaknesses of establish second-moment models (Launder *et al.* [9], Gibson and Launder [10]). As regards the last defect, Obi *et al.* have observed the separation streamline to double-up as the flow approaches the wall, reattaching at an angle of opposite sign to that of the streamlines in the shear layer remote from the wall.

While efforts are being made to rectify some of the aforementioned defects—for example, through non-linear pressure-strain models (Fu *et al.* [11]), improved corrective fragments accounting for wall-induced pressure reflections, anisotropy-sensitised forms of the equation governing turbulence-energy dissipation and even models for the individual components of the dissipation-rate tensor—there is a growing perception that second-moment closure is no panacea to all ills and is becoming excessively elaborate for the improvements in performance it aims to achieve. This has given impetus in the turbulence-modelling community to the formulation and application of formally simpler approaches based, broadly, on rational extensions of two-equation eddy-viscosity models.

The principal constraint inherent in linear eddy-viscosity models is the rigid 'local equilibrium' relationship between stresses and strains. Specifically, this linkage does not allow for stress-relaxation effects, and prevents the stress field from responding to vorticity. To overcome these limitations, several researchers have proposed anisotropic generalisations of the eddy-viscosity concept in conjunction with equations for turbulence energy and dissipation. Although most can be cast into a common mathematical form, their theoretical origins and derivations differ greatly. For example, the model of Yoshizawa [12] is based on the 'direct interaction approximation' (DIA), that of Speziale [13] is derived from continuum mechanical arguments, involving asymptotic expansions, and the variant of Rubinstein and Barton [14] arises from the 'renormalisation group' (RNG) theory of Yakhot and Orszag [15]. All relate, however, the Reynolds-stresses to mean strains by a second-order expression. A third-order low-Reynolds-number extension has recently been proposed by Craft *et al.* [16]. One novel feature of the last-named model is the use of strain and vorticity invariants to diminish the role of the turbulent Reynolds number and to suppress excessive energy generation through irrotational deformations.

It is possible to argue that the non-linear $k$–$\epsilon$ models are variants of the well-known algebraic stress model (ASM)—a simplified form of the Reynolds-stress-transport model which arises from the assumption that the ratio of each Reynolds-stress component to its transport term is isotropic. Indeed, this relationship is highlighted in a recent article by Gatski and Speziale [17]. However, there are significant differences between the two formulations. One is that the intimate link between any stress and its production terms, which is expressed in exact form by the Reynolds-stress equations, is not part and parcel of the non-linear eddy-viscosity model. Another is that the pressure-strain process is not treated and modelled as a separate physical mechanism on the basis of rational considerations linked to energy redistribution and isotropisation. While neither approach can be claimed to be 'superior' or 'inferior' relative to the other, it may be said that the ASM rests on a stronger fundamental basis which prescribes formally the physical coupling

between stresses and strains. This coupling is weaker in the non-linear $k$–$\epsilon$ model, a fact probably responsible for, among other weaknesses, the observed insufficient sensitivity of the stresses to swirl-related strains returned by this model.

Applications of non-linear eddy-viscosity models to separated flows are rare, and their performance in general conditions is, therefore, uncertain. Thangam and Speziale [18] have applied Speziale's form to a backward-facing-step flow and have demonstrated that the model returns a credible representation of anisotropy and a broadly correct reattachment location. However, the size of the secondary eddy in the step corner was under-estimated, and there were significant discrepancies between measured and computed velocity profiles, perhaps due to the dispersion effect of the convective fragments in the 'Oldroyd derivative' which is part of the model. Kobayashi and Togashi [19] have applied Yoshizawa's form to a similar geometry and have found that model to yield some, but by no means dramatic improvements relative to the linear $k$–$\epsilon$ model.

An entirely distinct approach to modelling turbulence has been taken by Yakhot and Orszag [15] who, using RNG theory, have essentially derived the $k$–$\epsilon$ model theoretically, without recourse to experimental data. The basic linear model does not, however, offer any advantages over the established form of Jones and Launder [20], unless combined with a correction to the $\epsilon$-equation recently proposed by Yakhot *et al.* [21]. That correction, not strictly arising from RNG considerations, is designed to sensitise the $\epsilon$-equation to high rates of strains so as to increase the rate of dissipation and thus lower the level of turbulent viscosity. A linear form of the model, as well as a non-linear variant in which the linear stress–strain relationship was replaced by Speziale's model with the convective fragments in the Oldroyd derivative neglected, have been applied by Yakhot *et al.* to a backward-facing-step flow [21]. While the linear RNG model has been demonstrated to return, in general, a better performance than the standard $k$–$\epsilon$ form, a correct representation of the size of the step-corner eddy and the shape of the recirculation zone could only be attained by use of Speziale's non-linear stress–strain relationship. Several reported applications of the linear RNG model to separated flow suggest that this model returns more extensive separation than that obtained from the standard $k$–$\epsilon$ model, but there is considerable uncertainty about the role of Yakhot *et al.*'s high-strain correction to the $\epsilon$-equation in this respect, and the model's capabilities cannot be judged as no detailed comparisons with experimental data for velocity and Reynolds stresses were reported.

The balance of experience derived from all studies suggests that it is important for any turbulence model—whatever its origin may be—to capture the disproportionate and inhomogeneous sensitivity of the stress components to secondary strains, especially those associated with curvature. In addition, any credible model must be able to account for redistribution processes at impingement/reattachment points and must be able to represent correctly the very different influence of rotational and irrotational strains on the stress fields. Yet another facet which is likely to affect model performance is the interaction between viscosity and the turbulence structure near the wall. While at very high Reynolds numbers this interaction will not greatly influence gross flow features, the sensitivity to this interaction can be expected to be marked as the Reynolds number declines. In particular, effects of viscous shear on the reattachment process may influence the size and shape of the recirculation zone.

The present paper aims to contribute to a clarification of the capability of different modelling strategies in representing the above interactions. Models investigated include linear and non-linear, standard and RNG $k$–$\epsilon$ variants as well as second-moment closure. Two non-linear $k$–$\epsilon$ models, namely Speziale's and Rubinstein and Barton's formulations, are tested. Two different wall-reflection fragments in Gibson and Launder's second-moment closure are examined to identify the origin of previously observed deficiencies in the predicted reattachment process. Finally, the authors' own low-Reynolds-number $k$–$\epsilon$ model (Lien and Leschziner, [22]) is also examined.

All above models and variants are applied to the backward-facing-step flow of Driver and Seegmiller, which is confined, following separation, by a 6° expanding channel. The Reynolds number, based on step height and maximum inlet velocity, is 36000.

In what follows, Section 2 summarises all turbulence models which feature in this study. Section 3 gives a brief description of the numerical procedure incorporating the models. In Section 4, results obtained with nine different turbulence-model variants were examined and compared with experimental data to identify the merits and weaknesses of the models. Finally, the outcome of the present investigation is summarised in Section 5.

## 2. TURBULENCE MODELS

### 2.1. Eddy-viscosity model

Based on series-expansion arguments, a general and co-ordinate invariant quadratic relationship between stresses and strains can be written as:

$$\overline{u_i' u_j'} = \tfrac{2}{3}k\delta_{ij} - \underbrace{\nu_T\left(\frac{\partial u_i}{\partial x_j} + \frac{\partial u_j}{\partial x_i}\right)}_{\text{linear term}} + \underbrace{\frac{k^3}{\epsilon^2}\left[C_{\tau 1}\left(\frac{\partial u_i}{\partial x_k}\frac{\partial u_j}{\partial x_k}\right)^* + C_{\tau 2}\left(\frac{\partial u_i}{\partial x_k}\frac{\partial u_k}{\partial x_j} + \frac{\partial u_j}{\partial x_k}\frac{\partial u_k}{\partial x_i}\right)^* + C_{\tau 3}\left(\frac{\partial u_k}{\partial x_i}\frac{\partial u_k}{\partial x_j}\right)^*\right]}_{\text{quadratic term}} \quad (1)$$

where '*' indicates the deviatoric part; for example:

$$\left(\frac{\partial u_i}{\partial x_k}\frac{\partial u_j}{\partial x_k}\right)^* = \frac{\partial u_i}{\partial x_k}\frac{\partial u_j}{\partial x_k} - \frac{1}{3}\frac{\partial u_m}{\partial x_n}\frac{\partial u_m}{\partial x_n}\delta_{ij} \quad (2)$$

In the conventional, linear formulation of the eddy-viscosity model, $C_{\tau 1}$, $C_{\tau 2}$ and $C_{\tau 3}$ are all zero. Two quadratic versions are investigated herein, namely those of Speziale† [13] and of Rubinstein and Barton [14]. These merely differ in respect of the numerical values of the coefficients. In Speziale's model,

$$(C_{\tau 1}, C_{\tau 2}, C_{\tau 3}) = (0.041, 0.014, -0.014), \quad (3)$$

while for Rubinstein and Barton's model,

$$(C_{\tau 1}, C_{\tau 2}, C_{\tau 3}) = (0.034, 0.104, -0.014). \quad (4)$$

The expanded 2D form of equation (1) in general curvilinear co-ordinates is given in Appendix A.

If the $k$–$\epsilon$ modelling framework is used, the eddy viscosity arises as:

$$\nu_T = C_\mu \frac{k^2}{\epsilon} \quad (5)$$

where $k$ and $\epsilon$ are determined from the conventional transport equations:

$$\frac{\partial u_i k}{\partial x_i} = \frac{\partial}{\partial x_i}\left[\left(\nu + \frac{\nu_T}{\sigma_k}\right)\frac{\partial k}{\partial x_i}\right] + P_k - \epsilon \quad (6)$$

$$\frac{\partial u_i \epsilon}{\partial x_i} = \frac{\partial}{\partial x_i}\left[\left(\nu + \frac{\nu_T}{\sigma_\epsilon}\right)\frac{\partial \epsilon}{\partial x_i}\right] + \frac{\epsilon}{k}(C_{\epsilon 1}P_k - C_{\epsilon 2}\epsilon) \quad (7)$$

with $P_k$ being defined as:

$$P_k = -\overline{u_i' u_j'}\frac{\partial u_i}{\partial x_j} \quad (8)$$

Different variants of the above model arise from the different approaches to determining the coefficients $C_\mu$, $\sigma_k$, $\sigma_\epsilon$, $C_{\epsilon 1}$ and $C_{\epsilon 2}$. Here, three forms are investigated, namely the high-Re $k$–$\epsilon$ model, the high-Re RNG $k$–$\epsilon$ model—both operating with log-law-based near-wall practices—and the authors' own low-Re $k$–$\epsilon$ model. The numerical values or expressions used in the above variants for the coefficients are as follows:

- Jones and Launder's model:

$$C_\mu = 0.09, \quad \sigma_k = 1, \quad \sigma_\epsilon = 1.3, \quad C_{\epsilon 1} = 1.44, \quad C_{\epsilon 2} = 1.92 \quad (9)$$

†The convective derivatives of the mean-velocity gradients are neglected here.

- Yakhot *et al.*'s RNG model:

$$C_\mu = 0.085, \quad \sigma_k = 0.72, \quad \sigma_\epsilon = 0.72$$

$$C_{\epsilon 1} = 1.42 - \frac{\bar{\eta}(1 - \bar{\eta}/4.38)}{1 + \beta\bar{\eta}^3}, \quad C_{\epsilon 2} = 1.68 \tag{10}$$

where

$$\beta = 0.012, \quad \bar{\eta} = \frac{Sk}{\epsilon}, \quad S = \sqrt{2S_{ij}S_{ij}}, \quad S_{ij} = \frac{1}{2}\left(\frac{\partial u_i}{\partial x_j} + \frac{\partial u_j}{\partial x_i}\right) \tag{11}$$

- Lien and Leschziner's model:

$$C_\mu = 0.09\left[\frac{1 - \exp(-0.016y^*)}{1 - \exp(-0.263y^*)}\right], \quad \sigma_k = 1, \quad \sigma_\epsilon = 1.3$$

$$C_{\epsilon 1} = 1.44\left(1 + \frac{P_k'}{P_k}\right), \quad C_{\epsilon 2} = 1.92[1 - 0.3\exp(-R_T^2)] - \underbrace{0.83\left(\frac{k^{3/2}/\epsilon}{2.44y} - 1\right)\left(\frac{k^{3/2}/\epsilon}{2.44y}\right)^2}_{\text{Yap's correction [23]}} \tag{12}$$

where $y^* = y\sqrt{k}/\nu$, $R_T = k^2/\nu\epsilon$ and

$$P_k' = \frac{1.92[1 - 0.3\exp(-R_T^2)]k^{3/2}}{3.53y[1 - \exp(-0.263y^*)]}\exp(-0.00222y^{*2}) \tag{13}$$

### 2.2. *Second-moment closure*

The transport equations for the Reynolds stresses may be written in the following Cartesian tensor form:

$$\frac{\partial u_k \overline{u_i' u_j'}}{\partial x_k} = D_{\overline{u_i' u_j'}} + \underbrace{P_{ij} + \Phi_{ij} - \tfrac{2}{3}\delta_{ij}\epsilon}_{S_{\overline{u_i' u_j'}}} \tag{14}$$

The conventional pressure-strain term $\Phi_{ij}$ combines Rotta's and the *Isotropisation of Production* proposals and related wall-corrections, i.e.

$$\Phi_{ij} = -C_1\frac{\epsilon}{k}(\overline{u_i' u_j'} - \tfrac{2}{3}\delta_{ij}k) - C_2(P_{ij} - \tfrac{1}{3}\delta_{ij}P_{kk}) + \Phi_{ij}^{\text{wall}} \tag{15}$$

in which

$$P_{ij} = -\left(\overline{u_i' u_k'}\frac{\partial u_j}{\partial x_k} + \overline{u_j' u_k'}\frac{\partial u_i}{\partial x_k}\right)$$

and

$$C_1 = 1.8, \quad C_2 = 0.6 \tag{16}$$

Two variants of wall-related pressure-strain fragments are adopted here, one being that normally used as part of Gibson and Launder's model [10], and the other a recent variation of Craft and Launder [24] which avoids the former's inappropriate near-wall enhancement of isotropisation at impingement/reattachment regions. Both forms can be written, collectively, as follows:

$$\begin{aligned}\Phi_{ij}^{\text{wall}} = {} & C_1'\frac{\epsilon}{k}(\overline{u_k' u_m'}n_k n_m\delta_{ij} - \tfrac{3}{2}\overline{u_i' u_k'}n_j n_k - \tfrac{3}{2}\overline{u_j' u_k'}n_i n_k)f \\ & - (C_2'\overline{u_k' u_m'} + C_3' k n_k n_m)\frac{\partial u_k}{\partial x_m}(n_q n_q\delta_{ij} - 3n_i n_j)f \\ & - C_4'(\tilde{\phi}_{km}n_k n_m\delta_{ij} - \tfrac{3}{2}\tilde{\phi}_{ik}n_j n_k - \tfrac{3}{2}\tilde{\phi}_{jk}n_i n_k)f\end{aligned} \tag{17}$$

where $n_i$ is the unit vector component in the $x_i$-direction, and the wall-proximity function $f$ is taken as directly proportional to the wall-normal distance with its coefficient chosen so that $f$ is unity in the log-law region. In the above, $\tilde{\phi}_{ij}$ takes the following alternative forms:

- Gibson and Launder's model:

$$\tilde{\phi}_{ij} = P_{ij} - \tfrac{1}{3}\delta_{ij}P_{kk}$$

$$C_1' = 0.5, \quad C_2' = 0, \quad C_3' = 0, \quad C_4' = 0.18 \tag{18}$$

- Craft and Launder's model:

$$\tilde{\phi}_{ij} = (\overline{u_i' u_k'} - \tfrac{2}{3}\delta_{ik}k)\frac{\partial u_j}{\partial x_k}$$

$$C_1' = 0.5, \quad C_2' = 0.08, \quad C_3' = 0.13, \quad C_4' = 0.10 \tag{19}$$

Since the above two variants of $\Phi_{ij}^{\text{wall}}$ are formulated in terms of Cartesian co-ordinates, it is necessary to consider carefully their validity and implementation in a general co-ordinate framework. This issue is addressed in Appendix B.

The transport equation for turbulence-energy dissipation, corresponding to equation (14), is as follows:

$$\frac{\partial u_k \epsilon}{\partial x_k} = D_\epsilon + \frac{\epsilon}{k}(0.5C_{\epsilon 1}P_{kk} - C_{\epsilon 2}\epsilon) \tag{20}$$

where

$$C_{\epsilon 1} = 1.44, \quad C_{\epsilon 2} = 1.92 \tag{21}$$

The diffusion of Reynolds-stresses, $D_{\overline{u_i u_j}}$, and dissipation rate, $D_\epsilon$, are conventionally approximated by Daly and Harlow's [25] generalised gradient diffusion hypothesis (GGDH):

$$D_{\overline{u_i u_j}} = \frac{\partial}{\partial x_k}\left(C_s \frac{k\overline{u_k' u_l'}}{\epsilon}\frac{\partial \overline{u_i' u_j'}}{\partial x_l}\right), \quad C_s = 0.22 \tag{22}$$

$$D_\epsilon = \frac{\partial}{\partial x_k}\left(C_\epsilon \frac{k\overline{u_k' u_l'}}{\epsilon}\frac{\partial \epsilon}{\partial x_l}\right), \quad C_\epsilon = 0.18 \tag{23}$$

This is one model used in computations to follow. It will be recognised, however, that this tensorial form gives rise, when expanded, to a number of cross-diffusion terms which turn out to be numerically destabilising—a problem which becomes particularly serious in 3D situations. This has motivated the replacement of equations (22) and (23) by a simplified, isotropic stress–diffusion model—a route previously adopted, for example, by Jones and Manners [26] and Lin [5].

If attention is focused on a plane homogeneous shear flow, the only non-zero diffusion process is normal to the flow. This allows an appropriate isotropic diffusivity to be obtained as:

$$C_\mu \frac{k^2}{\sigma_k \epsilon} \equiv C_s \frac{k\overline{v'^2}}{\epsilon}, \tag{24}$$

from which the Prandtl number for turbulence energy arises as:

$$\sigma_k = \frac{kC_\mu}{\overline{v'^2}C_s} \tag{25}$$

With $C_s = 0.22$ and $\overline{v'^2} \cong 0.361k$, the Prandtl number becomes 0.82. In the calculations to follow, the diffusivity for all Reynolds stresses has also been taken as that on the left-hand-side of equation (24). Similar arguments apply to $\sigma_\epsilon$, and these lead to:

$$\sigma_\epsilon = \frac{kC_\mu}{\overline{v'^2}C_\epsilon} \tag{26}$$

which here takes the value 1.0.

### 2.3. *Boundary conditions at wall*

The above second-moment closure is only applicable to high-Re-number flow and requires the use of a sub-model covering the semi-viscous near-wall layer. The calculations presented later have been obtained with the wall-function approach. This is based on the assumption that the turbulent near-wall region is described by the log law. Consistent with this are the following relations:

$$k = \frac{u_\tau^2}{\sqrt{C_\mu}}, \quad \epsilon = \frac{u_\tau^3}{\kappa y}, \quad \frac{\partial u}{\partial y} = \frac{u_\tau}{\kappa y}, \quad P_k = \epsilon \tag{27}$$

where $\kappa$ is the von Karman constant equal to 0.41 and $u_\tau$ $(=\sqrt{\tau_w/\rho})$ is the friction velocity.

For the non-linear $k$–$\epsilon$ model, the Reynolds stresses in the log-law region can be obtained by substituting equation (27) into (A1)–(A4) of Appendix A, yielding:

$$\overline{u'^2} = \left(\frac{2}{3} + \frac{2C_{\tau 1} - C_{\tau 3}}{3C_\mu}\right)k, \quad \overline{v'^2} = \left(\frac{2}{3} + \frac{2C_{\tau 3} - C_{\tau 1}}{3C_\mu}\right)k, \quad \overline{w'^2} = \left(\frac{2}{3} - \frac{C_{\tau 1} + C_{\tau 3}}{3C_\mu}\right)k, \quad -\overline{u'v'} = \sqrt{C_\mu}k \tag{28}$$

Hence, Speziale's model gives:

$$\overline{u'^2} = 1.022k, \quad \overline{v'^2} = 0.411k, \quad \overline{w'^2} = 0.567k, \quad -\overline{u'v'} = 0.300k \tag{29}$$

while for Rubinstein and Barton's model:

$$\overline{u'^2} = 0.990k, \quad \overline{v'^2} = 0.422k, \quad \overline{w'^2} = 0.588k, \quad -\overline{u'v'} = 0.291k. \tag{30}$$

In the case of second-moment closure, the Reynolds stresses obtained with Gibson and Launder's wall–reflection terms are:

$$\begin{aligned}
\frac{\overline{u'^2}}{k} &= \frac{4C_1 + 2C_1^2 - 4C_1C_2 + 2C_1C_4' + 6C_1' + 6C_1C_1' - 6C_2C_1'}{3C_1(C_1 + 2C_1')} = 1.098 \\
\frac{\overline{v'^2}}{k} &= \frac{2(-1 + C_1 + C_2 - 2C_4')}{3(C_1 + 2C_1')} = 0.247 \\
\frac{\overline{w'^2}}{k} &= 2 - \frac{\overline{u'^2}}{k} - \frac{\overline{v'^2}}{k} = 0.655 \\
\frac{-\overline{u'v'}}{k} &= \sqrt{\frac{2(1 - C_2 + 1.5C_4')(-1 + C_1 + C_2 - 2C_4')}{3(C_1 + 1.5C_1')(C_1 + 2C_1')}} = 0.255
\end{aligned} \tag{31}$$

while for Craft and Launder's alternative:

$$\begin{aligned}
\frac{\overline{u'^2}}{k} &= \frac{4C_1 + 2C_1^2 - 4C_1C_2 + 3C_1C_2' + 6C_1' + 6C_1C_1' - 6C_2C_1' - 4C_1'C_4'}{3C_1(C_1 + 2C_1')} = 1.071 \\
\frac{\overline{v'^2}}{k} &= \frac{2(-1 + C_1 + C_2 - 3C_2' - 2C_4')}{3(C_1 + 2C_1')} = 0.299 \\
\frac{\overline{w'^2}}{k} &= 2 - \frac{\overline{u'^2}}{k} - \frac{\overline{v'^2}}{k} = 0.7 \\
\frac{-\overline{u'v'}}{k} &= \sqrt{\frac{2(1 - C_2 - 1.5C_4')(-1 + C_1 + C_2 - 3C_2' - 2C_4')}{3(C_1 + 1.5C_1')(C_1 + 2C_1')} + \frac{C_4'}{C_1 + 1.5C_1'}} = 0.248
\end{aligned} \tag{32}$$

The above expressions have been derived by imposing the 'local equilibrium' conditions, equation (27), on the source term of the Reynolds-stress equations, $S_{\overline{u_i u_j}}$, in equation (14). The expanded 2D form of $S_{\overline{u_i u_j}}$ in curvilinear coordinates is given in Appendix C. For a curved wall, equations (27)–(32), applicable to a wall-oriented coordinate framework, need to be transformed in terms of Cartesian components, and these can be specified as boundary conditions for the Reynolds-stress equations.

In the case of Lien and Leschziner's low-Re $k$–$\epsilon$ model, $\epsilon$ at the node nearest to the wall is prescribed by:

$$\epsilon = \frac{0.75 P_k'}{1 - 0.3 \exp(-R_T^2)}, \tag{33}$$

which satisfies the following limiting value of $\epsilon$ at the wall:

$$\lim_{y \to 0} \epsilon = 1.56 \frac{\nu k}{y^2} \tag{34}$$

## 3. NUMERICAL SCHEME AND COMPUTATIONAL DETAILS

The present calculations were performed with a non-orthogonal, collocated, cell-centred finite-volume procedure, 'STREAM', recently developed at UMIST by Lien and Leschziner [27]. This method adopts the higher-order QUICK approximation (Leonard [28]) and the MUSCL/TVD scheme (van Leer [29]) to approximate advective volume-face fluxes, the latter applied, in scalar form, principally to the turbulence-model equations, including those of the linear/non-linear $k$–$\epsilon$ models and Reynolds-stress closure (Lien and Leschziner [30]). The solution is iterated to the steady state by means of a pressure-correction scheme, applicable to both incompressible and compressible (transonic) conditions (Lien and Leschziner [31]).

The numerical grids used to obtain the high-Re-model and low-Re-model solutions contained 110 × 60 and 110 × 80 grid lines, respectively; the grids are shown in Fig. 1 and also identify the geometry of the flow domain. These densities were selected on the basis of grid-independence tests with coarser grids. The next coarser levels investigated contained 85 × 45 and 100 × 70 grid lines, respectively. It is worth noting that the degree of support offered by the finest grids relative to the coarser ones is higher than suggested by the numerical ratios of grid lines, for the finest grids were arranged to cover a domain shortened from 32 to 24 step heights, and also because the additional transverse lines were arranged so as to give preferential support to the separated flow in the

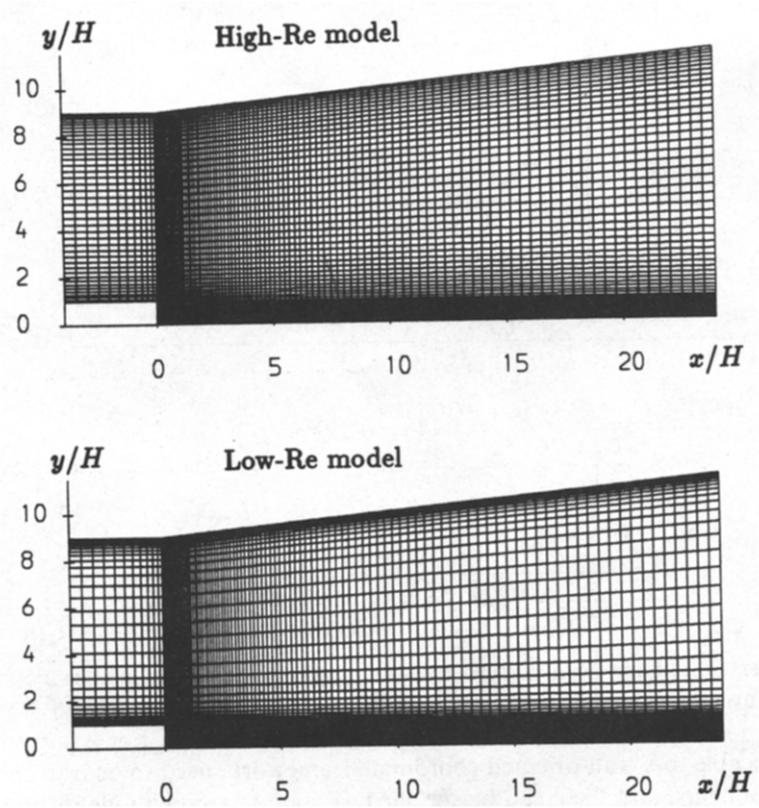


Fig. 1. Step geometry and numerical meshes.

vicininty of the step. Results for skin friction, wall pressure and velocity were found to display negligible grid-sensitivity for the two sets of grids identified above.

A solution was assumed to have converged when the sum of absolute cell residuals for mass and momentum, normalised by the respective inlet fluxes, fell below 0.1%. To achieve this state with the finest grids given above required between 1300 and 2200 iterations, depending on the turbulence model used. Execution times varied between 6 and 13 CPU minutes on a one-processor CRAY-YMP, the highest level of resource being required by the Reynolds-stress model.

## 4. RESULTS AND DISCUSSION

Results are presented for the nine model combinations identified in Section 2, three involving linear $k$–$\epsilon$ eddy-viscosity forms, three non-linear eddy-viscosity variants and three based on Reynolds-stress closure. The combinations are listed below, preceded by identifiers which are used in plots and the related discussion:

- STD $k$–$\epsilon$—Jones and Launder's model [defined by equation (9)]
- RNG $k$–$\epsilon$—Yakhot *et al.*'s model [defined by equations (10) and (11)]
- LL $k$–$\epsilon$—Lien and Leschziner's model [defined by equations (12) and (13)]
- N–L $k$–$\epsilon$/S—Speziale's model [defined by equation (3)]
- N–L RNG $k$–$\epsilon$/$S$—combining Speziale's and Yakhot *et al.*'s models [defined by equations (3), (10) and (11)]
- N–L RNG $k$–$\epsilon$/RB—combining Rubinstein and Barton's and Yakhot *et al.*'s models [defined by equations (4), (10) and (11)]
- RSTM–DH/$\Phi_{ijw}^{GL}$—standard Gibson and Launder's model [defined by equation (18)]
- RSTM–DH/$\Phi_{ijw}^{CL}$—Gibson and Launder's model combined with Craft and Launder's wall-reflection term [defined by equation (19)]

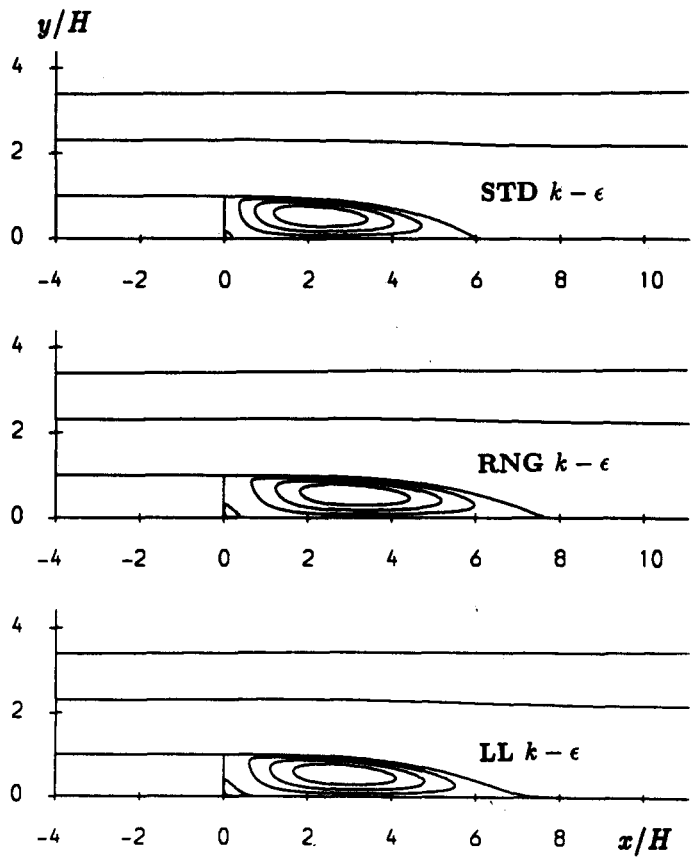


Fig. 2(a)—*caption overleaf.*

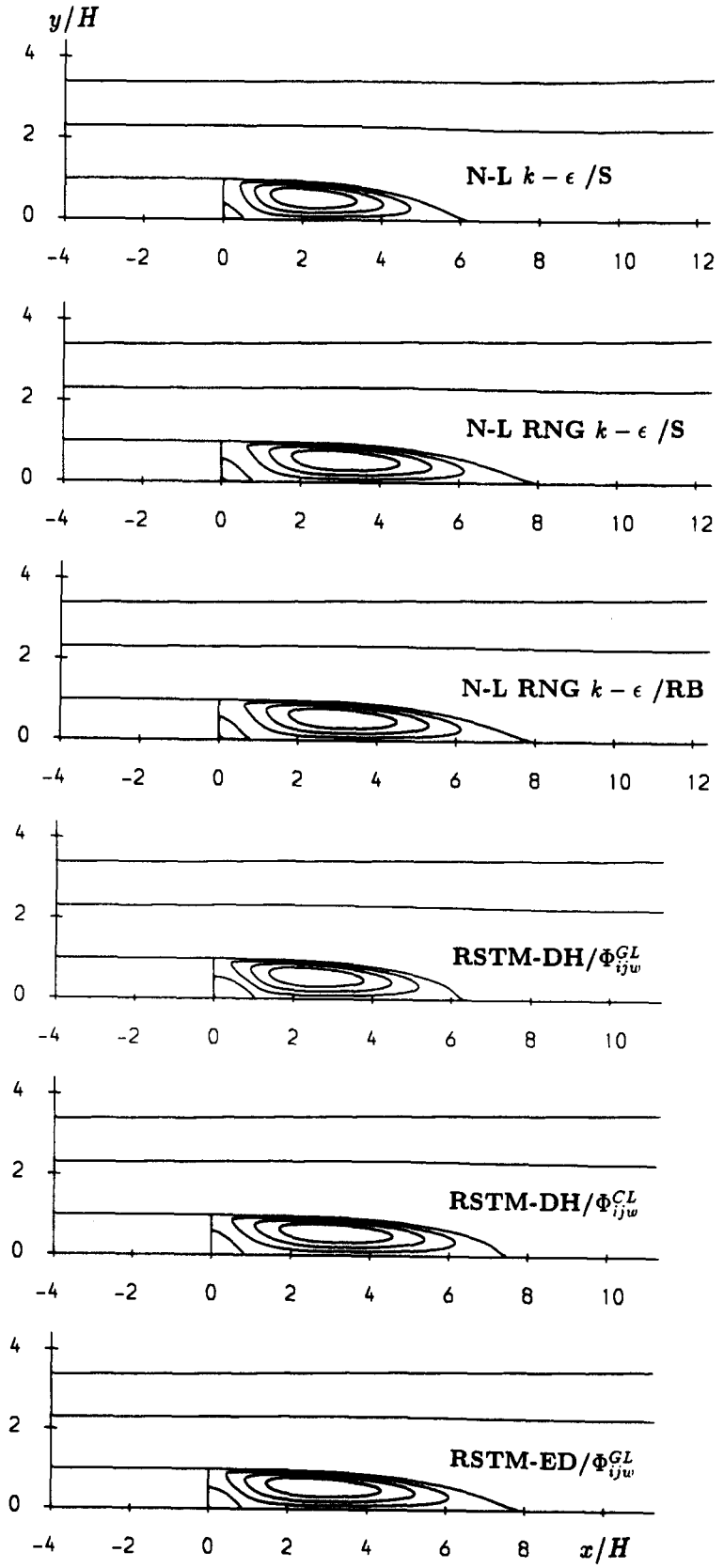


(b)

Fig. 2. Streamfunction contours in and around recirculation zone.

- RSTM–ED/$\Phi_{ijw}^{GL}$—Gibson and Launder's model combined with eddy-viscosity diffusion [defined by equations (25) and (26)]

An overall view of the response of gross flow features to turbulence-model variations is conveyed in Fig. 2 by stream-function plots of the recirculation zone. The experimental reattachment length, based on skin-friction measurements, is $8.2H$, and the measured variation of skin friction (to be considered later) suggests the existence of a secondary corner eddy of length $1H$. The worst result is returned by the standard $k$–$\epsilon$ model, while closest agreement is achieved with the non-linear RNG combination and the Reynolds-stress-transport model incorporating the isotropic stress–diffusion approximation.

Surprisingly, at first sight perhaps, is the sensitive response of the solution to the inclusion of low-Re processes. This sensitivity was initially thought to be partially linked to the very high resolution of the initial portion of the separated shear layer afforded by the very fine grid placed above the horizontal step wall upstream of the point separation. The need for this fine grid arose from the application of the low-Re model across the entire flow, including the boundary layer on the step wall. Within the present single-block (or single-mesh) approach, this highly dense grid extends into the separation region and results in a far higher resolution than that afforded by the grid employed in conjunction with wall functions. Some support for this suspicion was derived from the observation that the turbulence-energy level generated in the separated shear layer, close to the step, differed somewhat from that returned by the high-Re $k$–$\epsilon$ model. To resolve this ambiguity, the low-Re model was only applied downstream of the step, while the high-Re form was used upstream of the separation point. This application resulted in a solution very close to that included here. Hence, the sensitivity observed herein reflects model characteristics and is not contaminated by numerical error. More specifically, the sensitivity may reflect differences in the response of the respective $\epsilon$-equations to adverse pressure gradient. The present low-Re form was specifically constructed with the view to weakening the usual tendency of the $\epsilon$-equation to predict an inappropriate rise in the near-wall length scale in boundary layers subjected to adverse pressure gradient. This, and the inclusion of the length-scale correction by Yap [23] in the low-Re form, enhances a more realistic description of the reattachment process and hence results in an elongation of the recirculation bubble.

Introduction of the RNG $k$–$\epsilon$ form is also seen to yield in a not insignificant elongation of the recirculation zone, a result broadly in agreement with observations by others (e.g. Orszag *et al.* [32]). This elongation is due, principally, to the response of $C_{\epsilon 1}$ to the time-scale parameter $\bar{\eta}$. The value of $\bar{\eta}$ is preferentially elevated in the shear layer bordering the recirculation zone, thus increasing $C_{\epsilon 1}$. As a consequence, the dissipation rate rises and the turbulent viscosity is reduced. While this interaction is clearly beneficial in the present flow, it is found to be detrimental in others. Thus, the present authors have found the RNG form to return excessive rates of spread in plane and round jets and excessive separation in flow across a staggered tube-bank assembly (Leschziner and Launder [33]).

The inclusion of non-linear terms, defined by equation (1), to the stress–strain relation is seen to result in disappointingly small changes to the solution. In particular, the reattachment length remains almost unchanged relative to the standard linear $k$–$\epsilon$ model. The main benefit is an enlargement in the secondary corner eddy. Hence, when the non-linear proposal is combined with the RNG form—which, on its own, returns little change to the secondary eddy—the result is, as expected, a considerable elongation of the primary recirculation region as well as an enlargement of the secondary eddy. In fact, close examination reveals the presence of a tertiary corner eddy.

At the most complex level of second-moment closure, the predictive performance is seen to vary considerably, depending on the precise closure form used. All versions return a well-developed secondary eddy—a consequence of the reduction in turbulence transport, reflecting the ability of this type of closure to capture the interaction between curvature strain and the turbulent stresses. This interaction would be expected to be effective also in the curved shear layer bordering the recirculation zone. As will be demonstrated later, the process manifests itself by a reduction in shear stress in the inner portion of this layer, which tends to elongate the recirculation zone. However, it is evident from Fig. 2 that the recirculation length is also a sensitive

function of the model fragments approximating stress diffusion and wall-induced pressure–strain processes.

As pointed out earlier, the wall-reflection model in the Gibson–Launder closure returns a seriously erroneous increase in near-wall shear stress in response to the wall-normal strain associated with reattachment. It is this weakness which is responsible for the early reattachment observed in Fig. 2. Reversion to Craft and Launder's approximation results in a reattachment length in much closer agreement with experimental data.

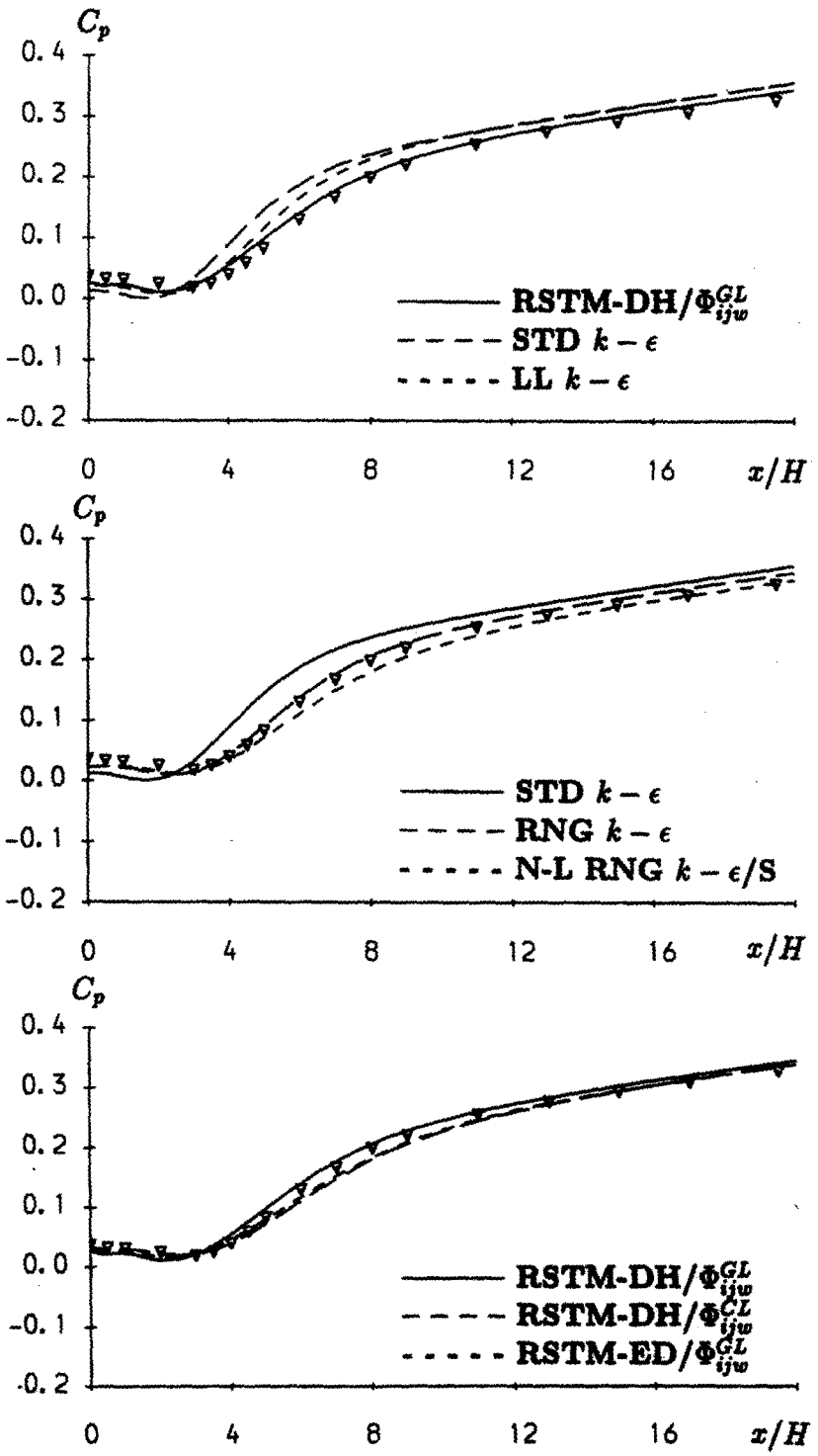


Fig. 3. Pressure-coefficient distributions.

The approximation of stress diffusion is not usually held to be very influential, but provokes a strong response in the present case. A closer examination of the stress field has revealed that this sensitivity originates, principally, from processes in the reattachment region where gradients of stresses vary rapidly. This statement is supported by the observation that the stream-function contour closest to the zero line (connecting separation to reattachment) is hardly affected by the diffusion model. Hence, the shift in the reattachment point is due to highly localised processes.

Variations of pressure and skin friction along the lower wall, corresponding to the stream function plots of Fig. 2, are shown in Figs 3 and 4, respectively. The former is particularly useful in identifying whether the *shape* of the recirculation region has been correctly captured, while the latter helps to identify the location of the primary and secondary eddies, and reflects the predictive accuracy of diffusive near-wall processes which are of special relevance in the context of heat transfer. Agreement between calculated and experimental pressure variations is seen to be close when the Reynolds-stress models and the RNG forms are used. Among these variants, those

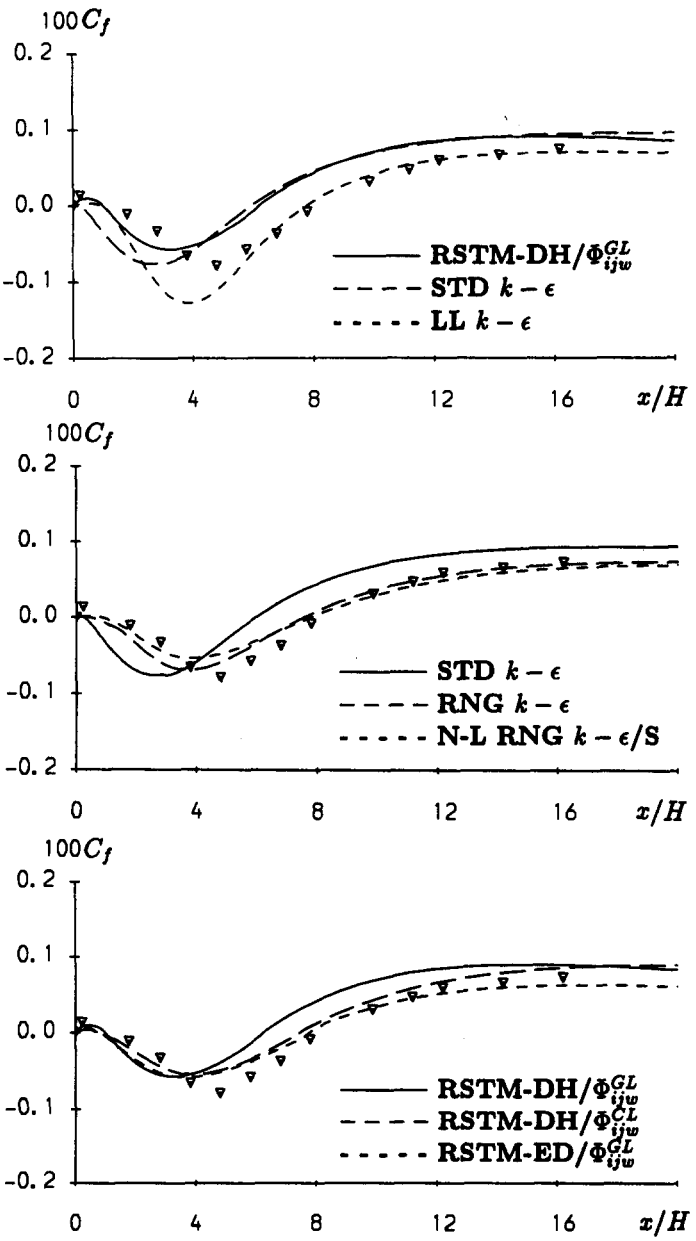


Fig. 4. Skin-friction distributions.

returning the longest attachment length, in best agreement with the experimental value, also predict the best variation of pressure within the range $0 < x < 8H$. Beyond reattachment, however, these same models are seen to return an insufficient rate of pressure recovery. This is a direct consequence of an insufficient rate of momentum recovery in the wake following reattachment, as will become clear later by reference to velocity profiles.

None of the models returns an entirely satisfactory representation of skin friction, but here too, those variants which perform best in relation to the shape of the recirculation zone also tend to

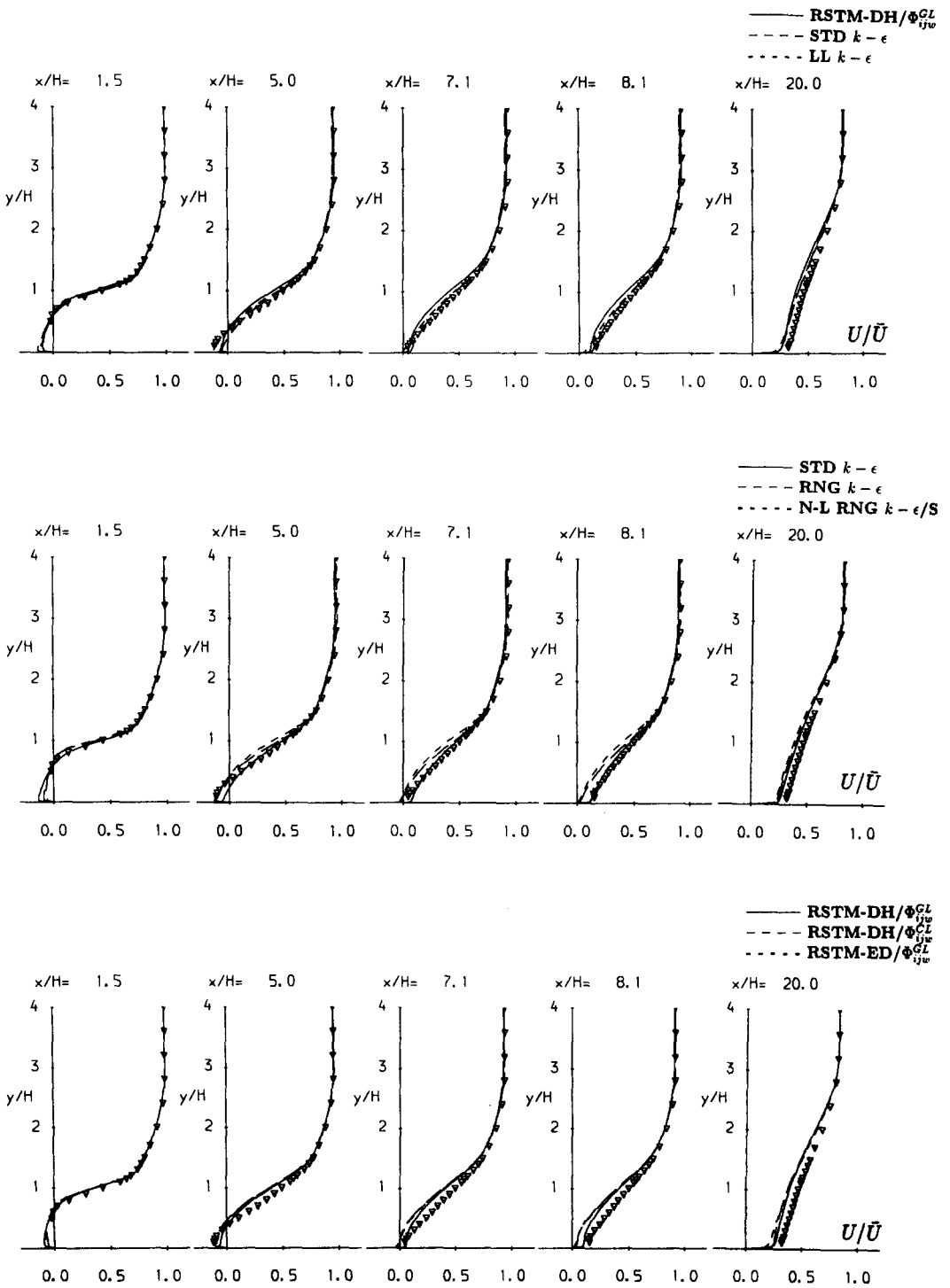


Fig. 5. Profiles of streamwise velocity.

do well in respect of frictional near-wall processes. For example, the standard $k$–$\epsilon$ model and the Gibson–Launder stress closure have earlier been observed to give particularly short recirculation zones, and these same models also return large discrepancies for skin friction. The latter model is seen, however, to capture well the effects of the secondary eddy and to give closer agreement within the separated zone as a consequence of the lower level of turbulence transport it returns in response to curvature.

Interestingly, the low-Re formulation predicts a seriously excessive level of (negative) skin friction within the separation zone. This might be assumed to indicate a large negative velocity near the wall. As will emerge later from a consideration of the velocity field, this is not, in fact, the cause. Rather, the main reason is that the state of turbulence in the recirculation zone is very far from being in equilibrium, being marked by very high levels of turbulence transport from the reattachment region towards the step. The low-Re model allows this high turbulence level to diffuse

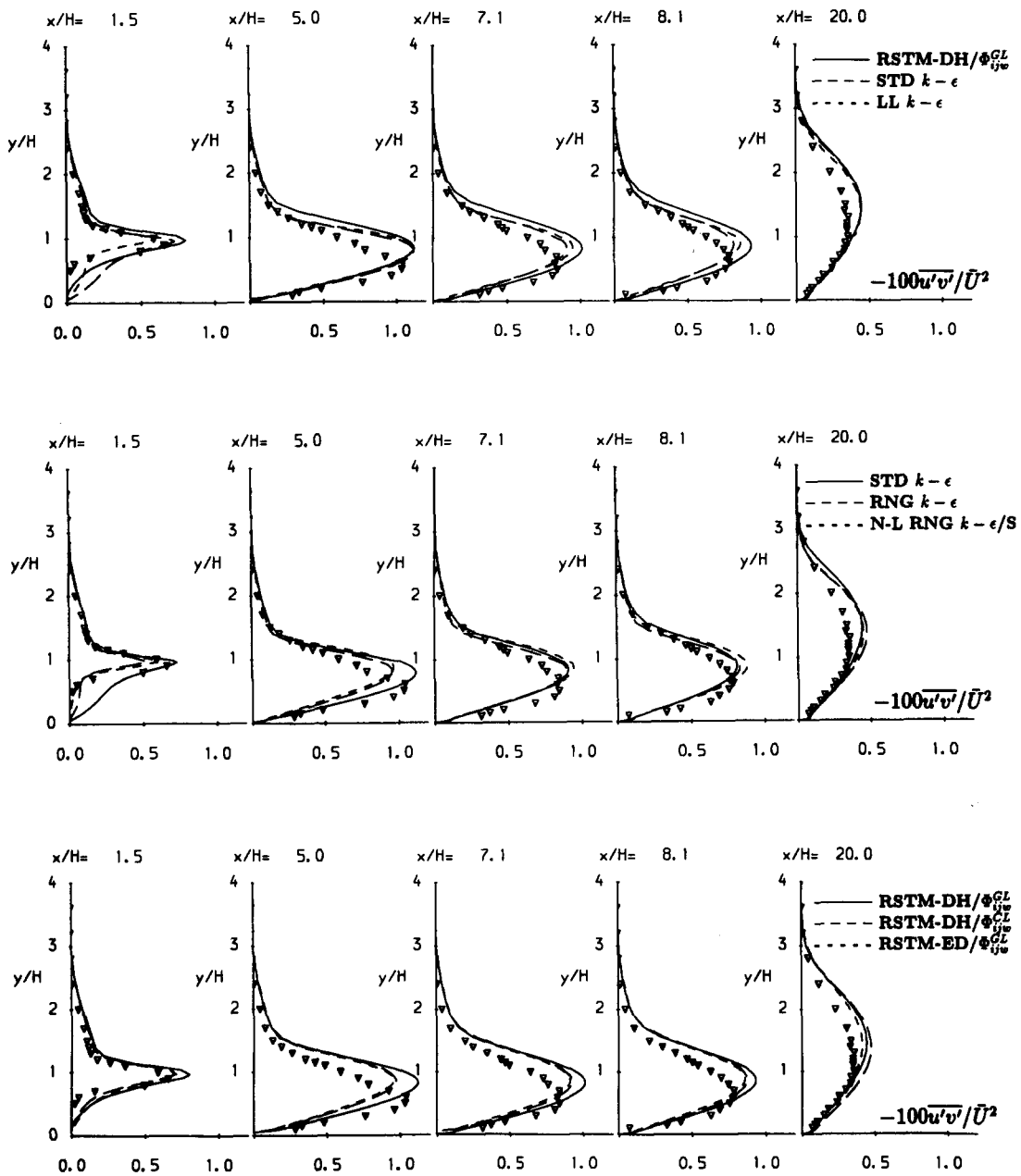


Fig. 6. Profiles of shear stress.

more readily towards the wall than does the log-law-based treatment, thus reducing the thickness of the viscous near-wall layer and increasing the wall shear stress.

Profiles of streamwise velocity at five locations covering the range $1.5 < x/H < 20$ are given in Fig. 5. At first sight, all models appear to return very similar distributions, but there are important differences as well as common defects. The standard $k$–$\epsilon$ model predicts, consistently with earlier observations, a rapid recovery resulting in early reattachment. The main reason is excessive diffusion in the curved shear layer bordering the recirculation zone—a defect manifesting itself by the insufficient level of shear strain in this area. In contrast, the recovery region appears to be represented particularly well by this model, but this is fortuitous and simply due to the premature reattachment obscuring a defect common to all models, namely an insufficient rate of momentum recover in the wake. Close examination of the profiles predicted by the low-Re model shows this variant to return a structure in the separated shear layer which is very similar to that predicted by its high-Re counterpart; the main difference lies in the near-wall behaviour, with the former model returning later reattachment and slightly higher reverse velocity, particularly close to the

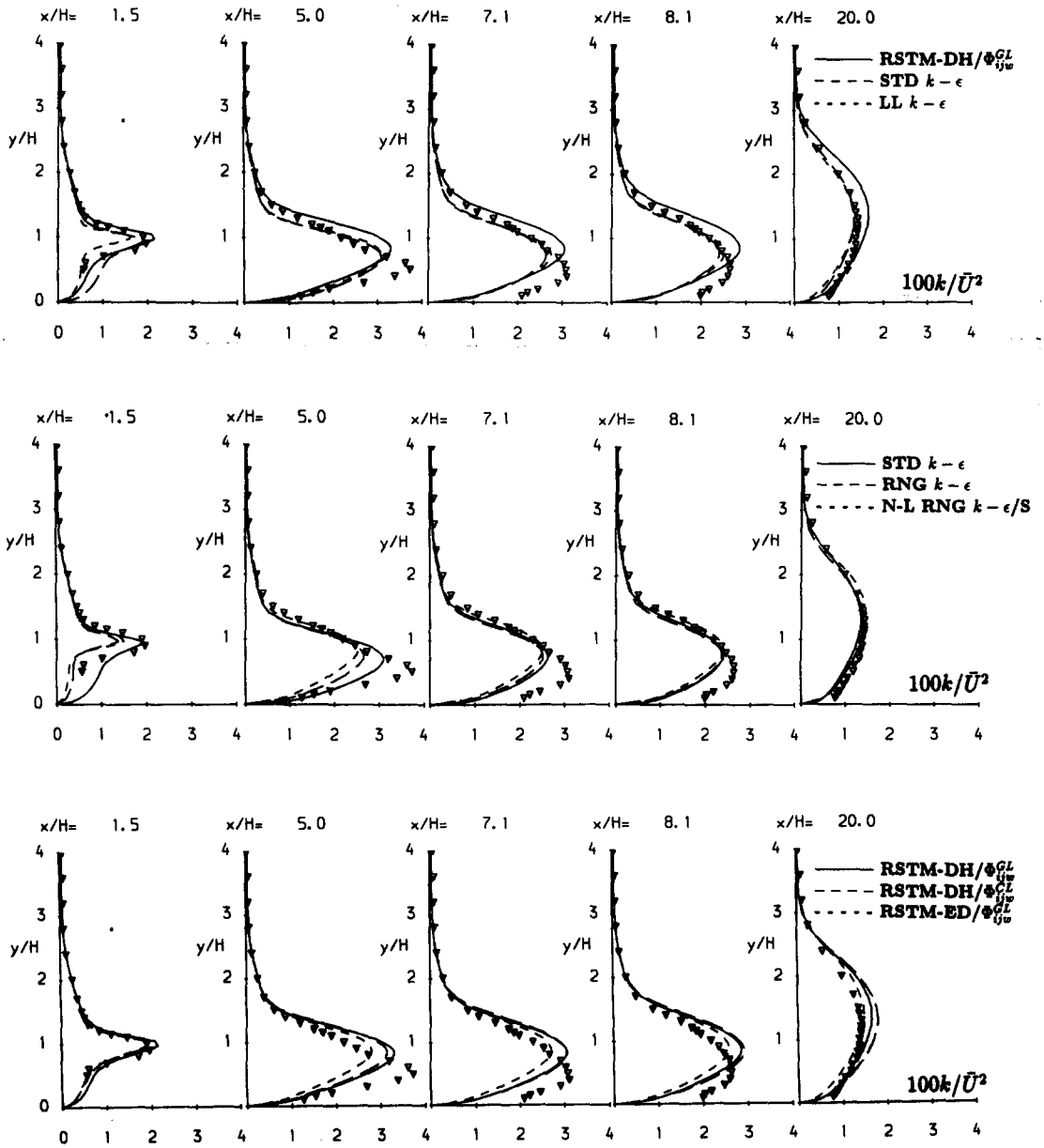


Fig. 7. Profiles of turbulence energy.

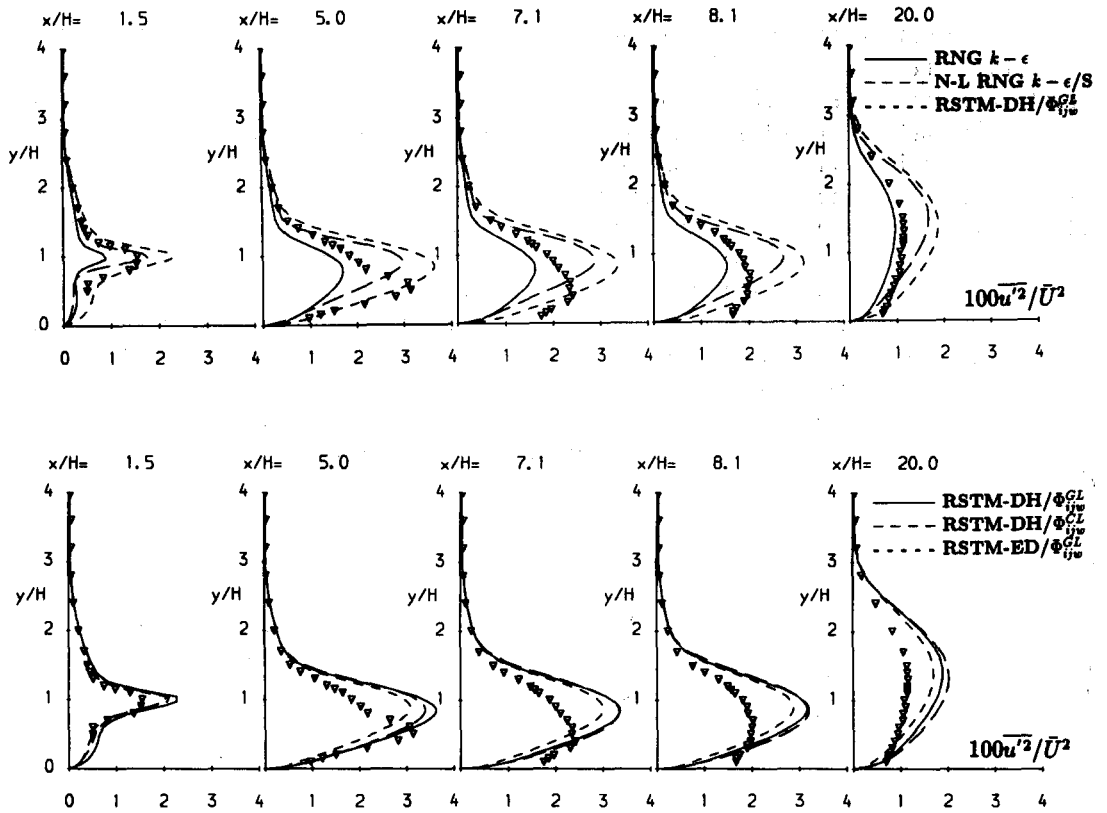


Fig. 8. Profiles of streamwise normal stress.

reattachment point. All other solutions share two common features: a better resolution of the free shear layer bordering the recirculation zone in the initial stages of development, coupled with an over-estimation of the shear strain further downstream, particularly in the wake region. There is a suggestion, based on the velocity data in wall proximity, that most models predict a delayed reattachment, and this brings to light a degree of inconsistency between the experimental variation of skin friction and the velocity profiles: the former suggests reattachment at $x = 8.2H$, while the velocity is clearly positive near the wall even at $x = 7H$. Hence, the assessment of the predictive qualities of any one model relative to others depends on precisely which subset of experimental data is judged to be more accurate.

The differences in the representation of the velocity field must clearly be rooted in variations in the predicted Reynolds-stress levels, and this relationship is explored by reference to Figs 6–9 which show, respectively, profiles of shear stress, turbulence energy and normal stresses, at the same locations as those for velocity. Solutions for shear stress and turbulence energy derived from the various models differ mainly within the recirculation zone, especially in the proximity of the step in the lower part of the recirculating bubble. Here, the RNG $k$–$\epsilon$ variants and the Reynolds-stress models, particularly the non-standard ones, give the lowest levels of stress and energy, consistent with the longest recirculation bubbles. Surprisingly, the low-Re $k$–$\epsilon$ model also returns significantly lower values of shear stress at $x/H = 1.5$. It is reasonable to suppose that the structure of the shear layer at this position should depend, principally, on the resolution of the boundary layer on the horizontal wall leading up to the step, and that this should, therefore, be largely insensitive to the variant of $k$–$\epsilon$ model used to compute the flow. On the other hand, however, the shear layer—even at an early stage of its development—can be expected to respond to processes within the recirculation zone, especially to the structure of the secondary eddy nesting in the step corner. As seen from Fig. 2, the low-Re model returns a considerably larger secondary eddy than the high-Re form, a sensitivity attributable to differences in the predicted response of the dissipation length scale to the pressure gradient, both at the reattachment point and at the step corner. Support for the argument linking the structure of the initial portion of the shear layer to the secondary corner eddy is given by the solutions returned by the RNG-modified linear and non-linear eddy-viscosity

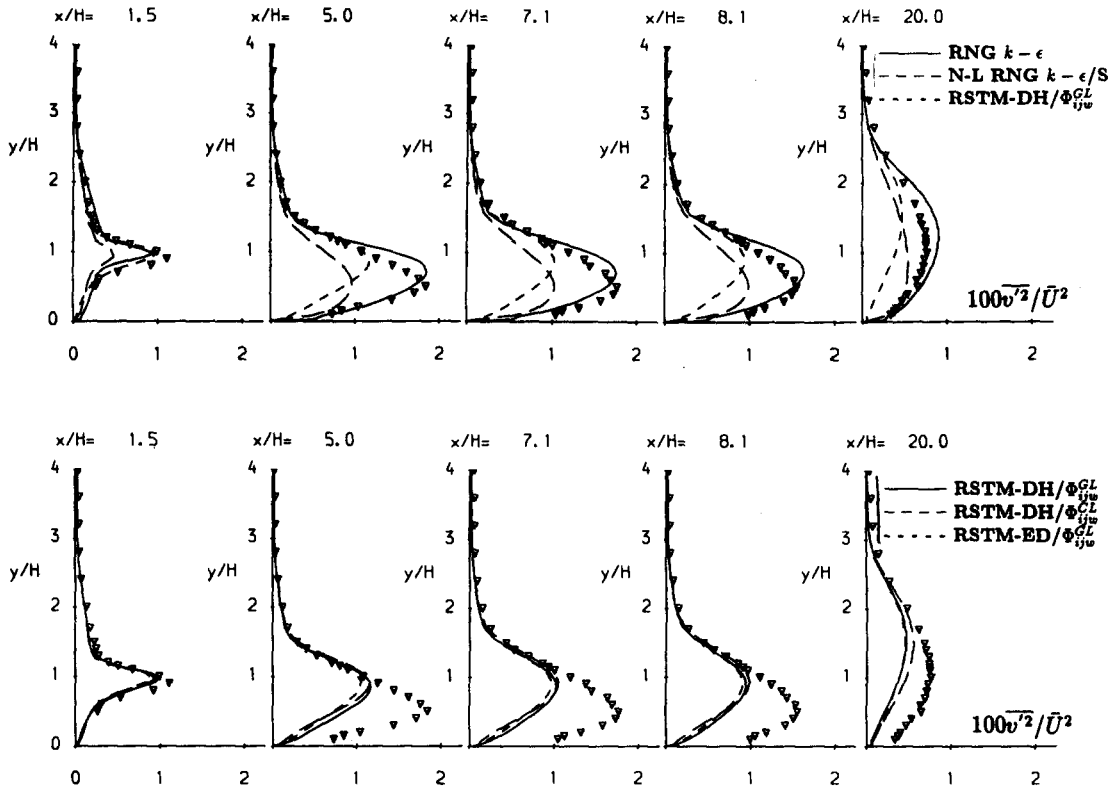


Fig. 9. Profiles of transverse normal stress.

models. Both variants give a wall-boundary-layer structure which is very close to that arising from the standard $k-\epsilon$ model, yet both also predict considerably lower shear stress and turbulence energy levels in the separated shear layer at $x/H = 1.5$.

A weakness shared by all solutions is that the positions of maximum shear stress and turbulence energy are too far away from the wall. With those models returning a broadly correct recirculation zone, this is accompanied by a second defect—perhaps indirectly provoking the first—namely an insufficient level of near-wall shear stress and turbulence energy. It is especially the latter discrepancy which is responsible for the insufficient rate of recovery in the wake and an upward shift of the position of maximum shear strain and hence turbulence generation.

Reference to Figs 8 and 9 reveals that the low level of near-wall shear is accompanied, in the case of the Reynolds-stress and non-linear eddy-viscosity models, by a seriously excessive degree of normal-stress anisotropy. The Reynolds–stress models return low values of wall-normal intensity in the near-wall region, and this causes, through generation, the low level of shear stress. In second-moment closure, anisotropy is dictated, principally, by a balance between generation and pressure–strain processes. Since the former is represented without formal approximation, defects in the predicted anisotropy must be due, mainly, to the latter process, the modelling of which is recognised to be very insecure. This is especially so in relation to effects arising from wall-induced pressure reflections. The fact that the wall-normal intensity is so low near the wall suggest that the present model fragments accounting for wall effects seriously over-estimate the decline of isotropisation as the wall is approached.

The non-linear eddy-viscosity model is seen to return a particularly poor representation of anisotropy. Here too, anisotropy is far too high, although the near-wall level of the wall-normal intensity is higher than that predicted by the Reynolds-stress closure and is hence closer to the experimental data. As the non-linear model embodies no explicit mechanism for wall-induced effects, this prominent difference in near-wall behaviour reinforces the earlier conclusion that the fragment representing pressure-reflection effects within the Reynolds-stress closure is too dominant. The observation that the non-linear model, which is derived along a very different formal route to that of second-moment closure, displays similar defects in respect of anisotropy is curious. It

is possible that the quadratic nature of the model, in terms of strains—a feature it shares with the second-moment variants used here, coupled with the calibration of the models by reference to turbulence energy and shear-stress levels for simple shear flows, unavoidably introduces common defects; this is an issue which remains to be examined more closely.

## 5. CONCLUSIONS

The predictive performance of several turbulence-closure proposals has been examined by way of comparisons between finite-volume solutions and experimental data for mean-flow quantities and Reynolds-stresses in a separated flow behind a backward-facing step followed by an expanding channel. The nine model variants investigated combined various fundamentally distinct approaches based on the traditional linear stress–strain $k$–$\epsilon$ eddy-viscosity formulation—both for high-Re and low–Re flow conditions, second-moment closure, the RNG approach and a non-linear stress–strain proposal.

It must be acknowledged first that the assessment is obscured, to some extent, by inconsistencies between wall-distributions of pressure and shear stress, on the one hand, and mean velocity, on the other. Specifically, skin-friction data suggest reattachment to occur at $x = 8.2H$, while the velocity profiles imply this location to be closer to $x = 7H$.

Based on wall distributions, Reynolds-stress closure, incorporating linear pressure–strain proposals, yields close agreement with the measured data only if combined with Craft and Launder's wall-reflection model or if Daly and Harlow's generalised-gradient-diffusion hypothesis is replaced by an isotropic-diffusion form. All second-moment-closure variants resolve well, in contrast to linear $k$–$\epsilon$ models (including the RNG version), the secondary corner eddy. To achieve a similar level of agreement with formulations other than those based on second-moment closure, the RNG formulation must be combined with a non-linear eddy-viscosity proposal.

An unexpected outcome of the study has been a marked sensitivity of the solution to the resolution of details in the semi-viscous near-wall layer by use of a low-Re $k$–$\epsilon$ model. Although numerical issues, specifically linked to grid-density differences in the separated shear layer, were originally thought to have contributed to this sensitivity, various numerical tests have confirmed that the differences in the solutions are rooted in model characteristics, particularly in respect of the predicted response of the dissipation length to pressure gradient.

Those models which perform best in relation to wall-distributions reveal most prominently a defect which is, essentially, common to all models, namely an insufficient rate of momentum recovery in the wake following reattachment. A related defect is that the location of maximum shear strain—and hence shear stress, turbulence energy and streamwise normal stress—is located too far away from the lower wall. In the case of second-moment closure, this appears to be due to excessive wall-induced damping of the wall-normal intensity, which leads, in turn, to an insufficient level of shear stress.

On the assumption that the experimental data for normal stresses are accurate, it may be stated that all models designed to resolve anisotropy return a poor representation of this property. In general, all models seriously over-estimate the level of anisotropy, implying fundamental defects in the pressure–strain proposals. The second-moment forms tend to return particularly low near-wall values, indicating additional defects in the model representing pressure-reflection effects on the pressure–strain process. The non-linear eddy-viscosity model is capable of resolving normal-stress anisotropy, in principle, but shows weaknesses which are even more serious than those returned by second-moment closure. The qualitative similarity between the defects displayed by the two modelling approaches, which follow quite different formalistic routes, suggests vaguely that the order to which a model relates stresses to strains, however formally effected, is of some significance to that model's predictive characteristics, at least in terms of anisotropy. The fact that all models are 'calibrated' by reference to simple shear flows, thus favouring close correspondence of the predicted shear-stress fields, may act to magnify common defects in the representation of anisotropy.

## REFERENCES

1. J. Kim, S. J. Kline and J. P. Johnston, Investigation of a recirculating turbulent shear layer: flow over a backward-facing step. *ASME J. Fluids Engng* **102**, 302 (1980).
2. J. K. Eaton and J. P. Johnston, Turbulent flow reattachment: an experimental study of the flow and structure behind a backward-facing step. Report MD-39, Thermo. Div., Dept of Mech. Engrg, Stanford University (1980).

3. D. M. Driver and H. L. Seegmiller, Features of a reattaching turbulent shear layer. AIAA Paper No. 82-1029 (1982).
4. M. Kadja, Computation of recirculating flow in complex geometries with algebraic second-moment closure. Ph.D. Thesis, Univ. of Manchester (1987).
5. C. A. Lin, Computations of three-dimensional injection into swirling flow with second-moment closure. Ph.D. Thesis, Univ. of Manchester (1990).
6. S. Sebag and P. Laurence, Reynolds stress transport model simulations of turbulent recirculating flows in complex domains. *Engineering Turbulence Modelling and Experiments 1* (Edited by W. Rodi and E. N. Ganic), p. 175. Elsevier Science Publishers (1990).
7. W. C. Lasher and D. B. Taulbee, Calculation of turbulent backstep flow: commentary on modelling of the pressure–strain correlation. *Engineering Turbulence Modelling and Experiments 1* (Edited by W. Rodi and E. N. Ganic), p. 195. Elsevier Science Publishers (1990).
8. S. Obi, M. Peric and G. Scheuerer, Second-moment calculation procedure for turbulent flows with collocated variable arrangement. *AIAA J.* **29,** 585 (1991).
9. B. E. Launder, G. J. Reece and W. Rodi, Progress in the development of a Reynolds-stress turbulence closure. *J. Fluid Mech.* **78,** 537 (1975).
10. M. M. Gibson and B. E. Launder, Ground effects on pressure fluctuations in the atmospheric boundary layer. *J. Fluid Mech.* **86,** 491 (1978).
11. S. Fu, B. E. Lander and D. P. Tselepidakis, Accommodating the effects of high strain rates in modelling the pressure–strain correlation. Report TFD/87/5, Dept of Mech. Engng, UMIST (1987).
12. A. Yoshizawa, Statistical analysis of the deviation of the Reynolds stress from its eddy viscosity representation. *Phys. Fluids* **27,** 1377 (1984).
13. C. G. Speziale, On non-linear $k$–$l$ and $k$–$\epsilon$ models of turbulence. *J. Fluid Mech.* **178,** 459 (1987).
14. R. Rubinstein and J. M. Barton, Non-linear Reynolds stress models and the renormalisation group. *Phys. Fluids A.* **2,** 1472 (1990).
15. V. Yakhot and S. A. Orszag, Renormalisation group analysis of turbulence: 1. Basic theory. *J. Sci. Comput.* **1,** 3 (1986).
16. T. J. Craft, B. E. Launder and K. Suga, Extending the applicability of eddy viscosity models through the use of deformation invariants and non-linear elements. *Proc. 5th Int. IAHR Symp. on Refined Flow Modelling and Turbulence Measurements*, Paris, France, p. 125 (1993).
17. T. B. Gatski and C. G. Speziale, On explicit algebraic stress models for complex turbulent flows. *J. Fluid Mech.* **254,** 59 (1993).
18. S. Thangam and C. G. Speziale, Turbulent separated flow past a backward-facing step: a critical evaluation of two equation turbulence models. NASA CR-187532 (1991).
19. T. Kobayashi and S. Togashi, Comparison of turbulence models applied to backward-facing step flow by LES data base. *Engineering Turbulence Modelling and Experiments 2* (Edited by W. Rodi and F. Martelli), p. 133. Elsevier Science Publishers (1993).
20. W. P. Jones and B. E. Launder, The prediction of laminarisation with a two-equation model of turbulence. *Int. J. Heat Mass Transfer* **15,** 301 (1972).
21. V. Yakhot, S. A. Orszag, S. Thangam, T. B. Gatski and C. G. Speziale, Development of turbulence models for shear flows by a double expansion technique. *Phys. Fluids A* **7,** 1510 (1992).
22. F. S. Lien and M. A. Leschziner, Computational modelling of 3D turbulent flow in S-diffuser and transition ducts. *Engineering Turbulence Modelling and Experiments 2* (Edited by W. Rodi and F. Martelli), p. 217. Elsevier Science Publishers (1993).
23. C. Yap, Turbulent heat and momentum transfer in recirculating and impinging flows. Ph.D. Thesis, Univ. of Manchester (1987).
24. T. J. Craft and B. E. Launder, New wall-reflection model applied to the turbulent impinging jet. *AIAA J.* **30,** 2970 (1992).
25. B. J. Daly and F. H. Harlow, Transport equation in turbulence. *Phys. Fluids* **33,** 1 (1970).
26. W. P. Jones and A. Manners. The calculation of the flow through a two-dimensional faired diffuser. *Turbulent Shear Flows 6*, Springer, p. 18 (1989).
27. F. S. Lien and M. A. Leschziner, A general non-orthogonal finite-volume algorithm for turbulent flow at all speeds incorporating second-moment closure, Part 1: Numerical implementation and Part 2: Application. *Comp. Meth. Appl. Mech. Eng.* 114, 123, 149 (1994).
28. B. P. Leonard, A stable and accurate convective modelling procedure based on quadratic upstream interpolation. *Comp. Meth. Appl. Mech. Eng.* **19,** 59 (1979).
29. B. van Leer, Towards the ultimate conservation difference scheme V, a second-order sequel to Godunov's method. *J. Comput. Phys.* **32,** 101 (1979).
30. F. S. Lien and M. A. Leschziner, Approximating turbulence convection in complex flows with a TVD-MUSCL scheme. *Proc. 5th Int. IAHR Symp. on Refined Flow Modelling and Turbulence Measurements*, Paris, France, p. 183 (1993).
31. F. S. Lien and M. A. Leschziner, A pressure–velocity solution strategy for compressible flow and its application to shock/boundary-layer interaction using second-moment turbulence closure. *ASME J. Fluids Engng* **115,** 717 (1993).
32. S. A. Orszag, V. Yakhot, W. S. Flannery, F. Boysan, D. Choudhury, J. Maruzewski and B. Patel, Renormalisation group modelling and turbulence simulations. *Near-Wall Turbulent Flows* (Edited by R. M. C. So, C. G. Speziale and B. E. Launder), p. 1031. Elsevier Science Publishers (1993).
33. M. A. Leschziner and B. E. Launder (Eds.), Round normally impinging turbulent jet and turbulent flow through tube bank sub-channel. *Proc. 2nd ERCOFTAC-IAHR Workshop on Refined Flow Modelling*, UMIST, Thermofluid Division (1993).

## APPENDIX A

The expanded 2D form of equation (32) in curvilinear coordinates is given below:

$$\overline{u'^2} = \tfrac{2}{3}k - 2\nu_T\frac{Du}{Dx} + \frac{k^3}{3\epsilon^2}\left[(C_{\tau 1}+2C_{\tau 2}+C_{\tau 3})\left(\frac{Du}{Dx}\right)^2 + (2C_{\tau 1}-C_{\tau 3})\left(\frac{Du}{Dy}\right)^2 + 2C_{\tau 2}\frac{Du}{Dy}\frac{Dv}{Dx} + (2C_{\tau 3}-C_{\tau 1})\left(\frac{Dv}{Dx}\right)^2\right] \quad \text{(A1)}$$

$$\overline{v'^2} = \tfrac{2}{3}k - 2\nu_T \frac{Dv}{Dy} + \frac{k^3}{3\epsilon^2}\left[(C_{t1}+2C_{t2}+C_{t3})\left(\frac{Du}{Dx}\right)^2 + (2C_{t3}-C_{t1})\left(\frac{Du}{Dy}\right)^2 + 2C_{t2}\frac{Du}{Dy}\frac{Dv}{Dx} + (2C_{t1}-C_{t3})\left(\frac{Dv}{Dx}\right)^2\right] \quad \text{(A2)}$$

$$\overline{u'v'} = -\nu_T\left(\frac{Du}{Dy}+\frac{Dv}{Dx}\right) + \frac{k^3}{\epsilon^2}(C_{t1}-C_{t3})\left(\frac{Du}{Dx}\frac{Dv}{Dx}+\frac{Du}{Dy}\frac{Dv}{Dy}\right) \quad \text{(A3)}$$

where

$$\frac{D\phi}{Dx} = \frac{1}{J}(\phi_\xi y_\eta - \phi_\eta y_\xi), \quad \frac{D\phi}{Dy} = \frac{1}{J}(-\phi_\xi x_\eta + \phi_\eta x_\xi), \quad \phi = u, v \quad \text{(A4)}$$

## APPENDIX B

In order to prove the validity of applying the wall-reflection fragments in $\Phi_{ij}$ in terms of curvilinear coordinates $(\xi, \eta)$, it is instructive to introduce the notation of stress transformation as follows:

$$[\tau] = [G]^T[\tau'][G] \quad \text{(B1)}$$

$$[\tau'] = [G][\tau][G]^T \quad \text{(B2)}$$

where the wall-oriented coordinates $\mathbf{e}'_i$ are related to their Cartesian counterpart $\mathbf{e}_j$ via:

$$\mathbf{e}'_1 = t_1\mathbf{e}_1 + t_2\mathbf{e}_2, \quad \mathbf{e}'_2 = n_1\mathbf{e}_1 + n_2\mathbf{e}_2. \quad \text{(B3)}$$

Then, the matrix $[G]$ is expressed as:

$$[G] = \begin{bmatrix} t_1 & t_2 \\ n_1 & n_2 \end{bmatrix}, \quad \text{(B4)}$$

Taking the *slow* part of $\Phi_{ij}^{\text{wall}}$,

$$\Phi_{ij,\text{slow}}^{\text{wall}} = C'_1\frac{\epsilon}{k}(\overline{u'_k u'_m}n_k n_m\delta_{ij} - \tfrac{2}{3}\overline{u'_i u'_k}n_j n_k - \tfrac{3}{2}\overline{u'_j u'_k}n_i n_k)f, \quad \text{(B5)}$$

as an example, the component $i = j = 1$ gives:

$$\Phi_{11,\text{slow}}^{\text{wall}} = C'_1\frac{\epsilon}{k}[(t_1^2 - 2n_1^2)(\overline{v'^2})' - 3t_1 n_1(\overline{u'v'})']f \quad \text{(B6)}$$

In recognition of $(t_1, t_2) \equiv (n_2, -n_1)$ from orthogonality, $(\overline{v'^2})'$ and $(\overline{u'v'})'$ in the above equation can be written by employing (B2) as:

$$(\overline{v'^2})' = n_1^2\overline{u'^2} + 2n_1 n_2\overline{u'v'} + n_2^2\overline{v'^2}, \quad \text{(B7)}$$

$$(\overline{u'v'})' = n_1 n_2(\overline{u'^2} - \overline{v'^2}) + (n_2^2 - n_1^2)\overline{u'v'}. \quad \text{(B8)}$$

Substituting (B7) and (B8) into (B6) in conjunction with the requirement $n_1^2 + n_2^2 = 1$ for a unit vector, (B6) is further simplified to:

$$\Phi_{11,\text{slow}}^{\text{wall}} = C'_1\frac{\epsilon}{k}[-2n_1^2\overline{u'^2} + n_2^2\overline{v'^2} - n_1 n_2\overline{u'v'}]f, \quad \text{(B9)}$$

which is exactly the same as the expression expanded with (B5) in term of Cartesian Reynolds-stress components $\overline{u'_i u'_j}$. Similar proofs can be derived for $\Phi_{22,\text{slow}}^{\text{wall}}$ and $\Phi_{12,\text{slow}}^{\text{wall}}$ without any difficulty. Analogous arguments also apply to the *rapid* part of $\Phi_{ij}^{\text{wall}}$ if it is assumed that $\tilde{\phi}_{ij}$ is proportional to $\overline{u'_i u'_j} - \frac{2}{3}\delta_{ij}k$. Hence, the $\Phi_{ij}^{\text{wall}}$ of Gibson and Launder's and Craft and Launder's variants, when expressed by forms corresponding to equation (17), applies to curved walls.

## APPENDIX C

The expanded 2D form of equation (14) for $S_{\overline{u_i u_j}}$ $(= P_{ij} + \Phi_{ij} - \frac{2}{3}\delta_{ij}\epsilon)$ in curvilinear coordinates is given below:

$$\begin{aligned} S_{\overline{u'^2}} = {} & \frac{\epsilon}{k}[-(C_1 + 2C'_1 f_{xx})\overline{u'^2} + C'_1 f_{yy}\overline{v'^2} - C'_1 f_{xy}\overline{u'v'}] \\ & + (1 - C_2)P_{11} + [\tfrac{2}{3}C_2 + C'_2(f_{yy} - 2f_{xx})]P_k + \tfrac{2}{3}(C_1 - 1)\epsilon \\ & + C'_3 k\left[\frac{Du}{Dx}(3f_{xxxx} - f_{xx}) + \frac{Dv}{Dy}(3f_{xyxy} - f_{yy}) + \left(\frac{Du}{Dy} + \frac{Dv}{Dx}\right)(3f_{xyxx} - f_{xy})\right] \\ & + C'_4[2\tilde{\phi}_{11}f_{xx} - \tilde{\phi}_{22}f_{yy} + (2\tilde{\phi}_{21} - \tilde{\phi}_{12})f_{xy}] \end{aligned} \quad \text{(C1)}$$

$$\begin{aligned} S_{\overline{v'^2}} = {} & \frac{\epsilon}{k}[-(C_1 + 2C'_1 f_{yy})\overline{v'^2} + C'_1 f_{xx}\overline{u'^2} - C'_1 f_{xy}\overline{u'v'}] \\ & + (1 - C_2)P_{22} + [\tfrac{2}{3}C_2 + C'_2(f_{xx} - 2f_{yy})]P_k + \tfrac{2}{3}(C_1 - 1)\epsilon \\ & + C'_3 k\left[\frac{Dv}{Dy}(3f_{yyyy} - f_{yy}) + \frac{Du}{Dx}(3f_{xyxy} - f_{xx}) + \left(\frac{Du}{Dy} + \frac{Dv}{Dx}\right)(3f_{xyyy} - f_{xy})\right] \\ & + C'_4[2\tilde{\phi}_{22}f_{yy} - \tilde{\phi}_{11}f_{xx} + (2\tilde{\phi}_{12} - \tilde{\phi}_{21})f_{xy}] \end{aligned} \quad \text{(C2)}$$

$$
\begin{aligned}
S_{\overline{u'v'}} = & -\frac{\epsilon}{k}\{[C_1 + 1.5C_1'(f_{xx}+f_{yy})]\overline{u'v'} + 1.5C_1' f_{xy}(\overline{u'^2}+\overline{v'^2})\} \\
& + (1-C_2)P_{12} - 3C_2' f_{xy} P_k \\
& + 3C_3' k\left[\frac{Du}{Dx} f_{xyxx} + \frac{Dv}{Dy} f_{xyyy} + \left(\frac{Du}{Dy}+\frac{Dv}{Dx}\right) f_{xyxy}\right] \\
& + 1.5C_4'[\tilde{\phi}_{12} f_{xx} + \tilde{\phi}_{21} f_{yy} + (\tilde{\phi}_{12}+\tilde{\phi}_{12}) f_{xy}]
\end{aligned} \tag{C3}
$$

where

$$
\begin{aligned}
& f_{xx} = n_1 n_1 f \quad f_{yy} = n_2 n_2 f \quad f_{xy} = n_1 n_2 f \\
& f_{xxxx} = n_1^4 f \quad f_{yyyy} = n_2^4 f \\
& f_{xyxx} = n_1 n_2 n_1^2 f \quad f_{xyyy} = n_1 n_2 n_2^2 f \quad f_{xyxy} = (n_1 n_2)^2 f \\
& f = \frac{k^{3/2}/\epsilon}{2.45\Delta n}
\end{aligned} \tag{C4}
$$

and $D\phi/Dx$ and $D\phi/Dy$ are defined in (A4).